5. PLASMA ENGINEERING SYSTEMS AND TOOLS FOR FUSION DEVICES

C.A.F. Varandas (Head), P. Amorim, J.P. Bizarro, C. Correia, C. Loureiro, I. Nedzelkij, A. Batista, B.B. Carvalho, P. Coelho, A. Combo, M. Correia, M. Cunha, A. Figueiredo, R. Gomes, B. Gonçalves, A. Palmeirinha, J. Pereira, A. Rodrigues, J. Sousa

5.1. INTRODUCTION

This project aims at developing of plasma engineering systems, data analysis methods and plasma physics studies based on the experimental results obtained with the developed diagnostics. In 2000, the project included the following research lines:

- X-ray diagnostics for TCV
- Distributed system for fast timing and event management on MAST
- Heavy ion beam diagnostic for the TJ-II stellarator
- Laser induced fluorescence diagnostic for TJ-II
- Digital instrumentation for control and data acquisition
- Wigner distributions for time-frequency analysis of fusion plasma signals

5.2. X-RAY DIAGNOSTICS FOR TCV

The following main activities were carried out during 2000:

- Operation of the equatorial Pulse Height Analysis (PHA) spectrometer
- Development of software for the routine analysis of the diagnostic data
- Alterations on the PHA diagnostic to extend the detected energy range from soft to hard X-ray region.
- Shielding of the detector with lead
- Installation of a new collimator with variable aperture aiming at to control the incoming X-ray flux.
- Design and construction of a new mechanical support structure of the detector assembly in order to held the extra weight required by the new lead shielding.
- Development of MATLAB routines to extract the Thomson scattering data and to compare the electron temperatures obtained with both diagnostics.
- Evaluation in Lisbon of a rotating crystal spectrometer lent by the Princeton Plasma Physics Laboratory
- Repair of the protection components of the detectors and testing of the vacuum chamber
- Definition of the characteristics of a step-by-step motor and a high voltage power supply for this new diagnostic.

5.3. DISTRIBUTED SYSTEM FOR FAST TIMING AND EVENT MANAGEMENT ON MAST

5.3.1. Introduction

The following main tasks have been performed:

- Laboratorial tests of eleven VME modules
- Development of software for testing and operation
- Implementation, testing and operation of the VME system on the MAST tokamak
- Re-programming of the Field Programmable Gate Array (FPGA) of the timing unit aiming at the utilization of the VME system in discharges lasting up to 100 seconds.
- End of the design of the circuit of the CAMAC version of the Event and Pulse Node (EPN) module.
- Commissioning of the CAMAC version of the EPN module, including the design, simulation and testing of a CAMAC interface FPGA.
- Development of software for the CAMAC version.

5.3.2. Tests of the EPN timing unit

The Timing Unit (TU) of the EPN module was tested aiming at verifying the correct operation of the output/input channels. By designing an experimental set-up and providing defined parameters, it was possible to test most typical and boundary conditions that may occur in real operation.

The tests that have been carried out present typical conditions and representative frames allowing extrapolation of the behaviour of all other frames. This conclusion is possible due to architectural considerations and it is very important because is impossible to test all frames. Boundary conditions received a very thorough attention to prevent unspecified situations during transitions between frames or between operation modes.

Fig. 5.1 depicts the results of one representative test.

The results of the TU tests are presented in a report, providing an accurate definition of the occurrence time of each signal in the outputs, which allows the implementation of the correct software routines for the global data acquisition time stamping.

5.3.3. Software

Two CDs have been authored and set-up programs were designed to easily send and install the Trigger and Timing System (TTS) packages. These CDs contains:

A. Cygwin Development Environment

- Cygwin
- GTK+, GLADE
- Integrated Development Environment

B. TTS Design Platform

- GEPN for Win32
- OS-9 Drivers
- OS-9 EPN test program
- GEPN for Hawk
- TTS Documents
- EPN Hardware Design Files
- Reflector Hardware Design Files
- FAN-IN (OUT) Hardware Design Files

This section contains the description of two software programs: GEPN and the OS-9 drivers.

GEPN is the interface software that allows the remote programming of the configuration of the timing system in a per node base. It allows to program the trigger times, trigger edge, gate widths, sample frequencies, number of samples in each section of a timing train, global event/triggers definition, digital signal input/output, real-time operation and includes an event log viewer. The timing system can then be tested node by node autonomously from the global data acquisition system.

Fig. 5.2 shows one window of the user-friendly interface.

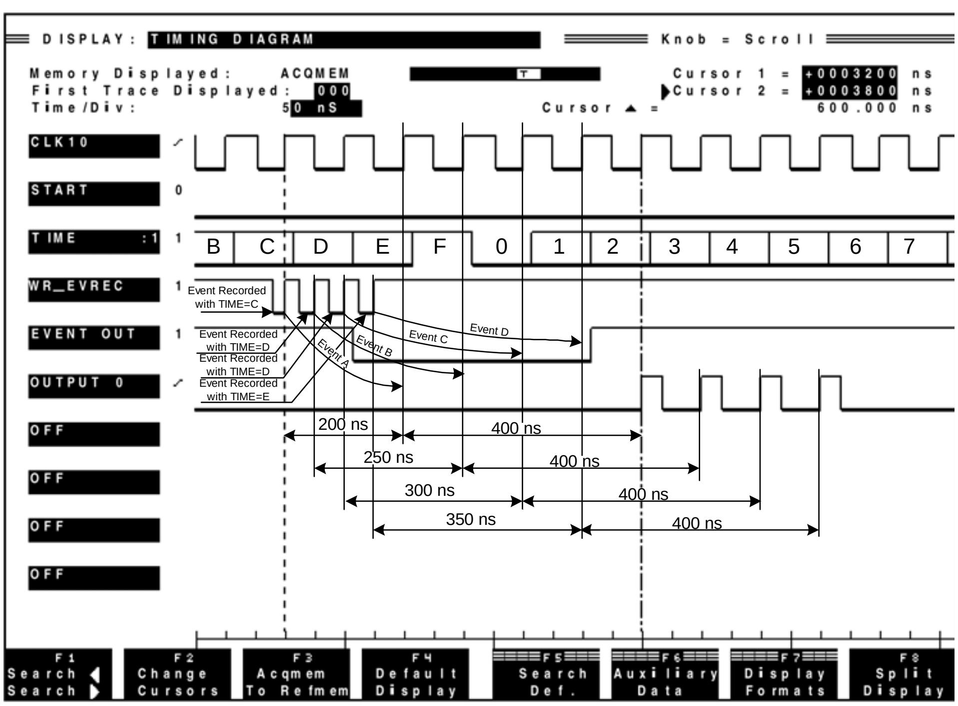

Fig. 5.1 – Event recording operation

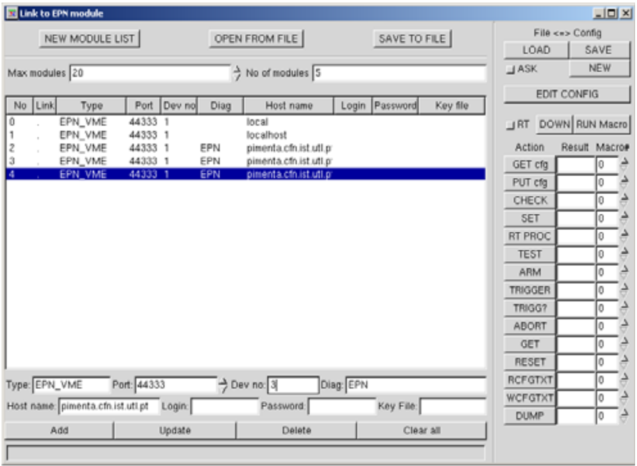

Fig. 5.2 – GEPN remote node and action selection window

The configuration may also be forwarded to the central data acquisition system, stored in the database and passed to the concerned modules before each tokamak discharge. Each diagnostic have its own database, and the overall controller of the data acquisition process links the databases for the different diagnostics.

GEPN was designed with graphical display architecture and the C code is portable to several computers platforms including Win32, Linux and other. Design and compilation was made with the GNU licensed GTK+ graphical libraries and the GLADE interface designer, both in-house ported to the Cygwin for Win32 platform.

Fig. 5.3 depicts an example of the window design with GLADE.

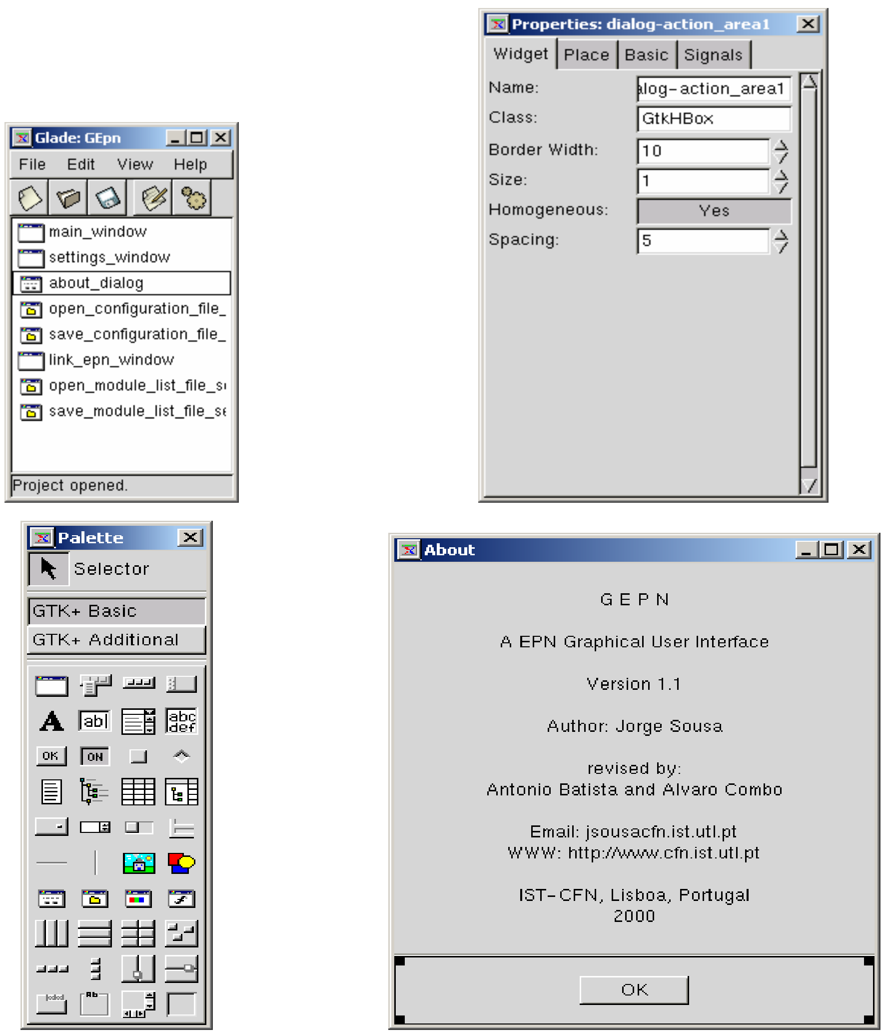

Fig. 5.3 – GLADE window designer

The OS-9 EPN device drivers allow the data acquisition system to load parameters into the timing system prior to the experimental shot and to retrieve data from the system after a shot is completed. They also enable the functionality of the system to be verified at subsystem level and as a full operating system.

The drivers were designed in order to support both the CAMAC and VME versions of the EPN and include the:

(i) CDAS Trap handler
(ii) EPN low-level access routines
(iii) EPN register port access and interrupt handle
(iv) CDASD network daemon

5.4. HEAVY ION BEAM DIAGNOSTIC FOR TJ-II

5.4.1. Introduction

The following main activities were made during this year:

- Improvement of the dedicated control and data acquisition system
- Collaboration on the implementation and beginning of operation of the ion injector and electrostatic energy analyser
- Design of a new version of the trans-impedance amplifier, aiming at to increase the bandwidth and to reduce the noise
- Implementation of a first multiple cell array detector (MCAD)
- Preliminary studies of filters for the MCAD, aiming at the reduction of the noise due to the plasma radiation.
- Study of a modified biased split detector for the electrostatic energy analyser

5.4.2. Modified biased split detector

Measurements of the plasma potential by a heavy ion beam diagnostic (HIBD) require an accuracy $\Delta E/E_b \leq 10^{-4}$, which on the electrostatic energy analysers is provided by the differential detection of the ion beam on the split detector. The actual currents on the split detector are a combination of both the ion and electron currents. The uniform secondary electron emission from the split detector does not influence the analyser operation. However, the different geometry and surface conditions of the split plates and the asymmetric secondary electrons exchange between the plates (for example, due to stray magnetic field of a plasma device existing in the vicinity of the detector) break the uniformity of the secondary electron flux and can strongly disturb the measurements.

The presence of the secondary electrons effect can be identified by the analysis of the dynamic curve:

$$(ND) = (i_t - i_b)/(i_t + i_b) = \delta\tilde{i} = f(U_b + \Phi_{pl})/2U_a. \quad (5.1)$$

In an ideal case it should be linear and symmetrically saturated on ±1 (Fig. 5.4) The point where (ND) = 0 is determined by the top-bottom currents equality. The shift of this point on the beam energy scale determines the values of the plasma potential. Shifts associated with any other effects, except that of the plasma potential, indicate the error introduced into the measurements. The error due to secondary electrons in general is given by:

$$\Delta U = \tfrac{1}{2}\{[\alpha_b(1+\beta_b)-\alpha_t(1+\beta_t)+2k(\beta_b-\beta_t)]/[\alpha_t(1+\beta_t)+\alpha_b(1+\beta_b)+2]\}\Delta U_d \quad (5.2)$$

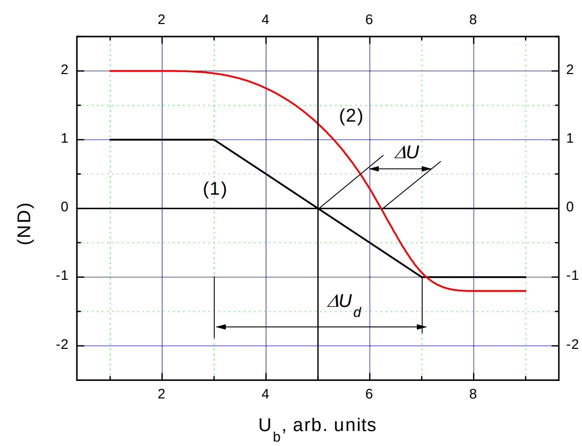

Fig. 5.4 - Ideal (1) and modified by secondary electrons (2) dynamic curves of the split detector.

where α_t, α_b and β_t, β_b are the respective secondary electron emission and electron exchange coefficients on top and bottom split plates, $k = i_{uv}/i_{beam}$ is the inverse signal-to-noise ratio of the detector with a noisy signal of uniform secondary electron flux created by the plasma UV radiation, and $\Delta U_d = 4FU_a$ is the dynamic range of the energy analyser. The estimations obtained with equation (5.2), using the existing experimental data, show that the error can be of the order of the measured plasma potential.

A modified biased split detector has been elaborated in collaboration with IPP, Kharkov, Ukraine, for the full suppression of the secondary electrons (Fig. 5.5).

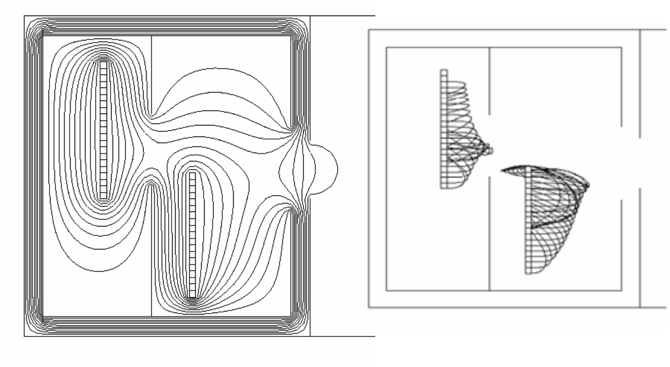

Fig. 5.5 – Lines of equal potential (100 V on electroddes) (a) and trajectories of the 4 eV secondary electrons (b) of the bias detector with full suppression of secondary electrons.

The experimental dynamic curve of the electrostatic energy analyser with this detector is shown in Fig. 5.6 and demonstrates its excellent performance.

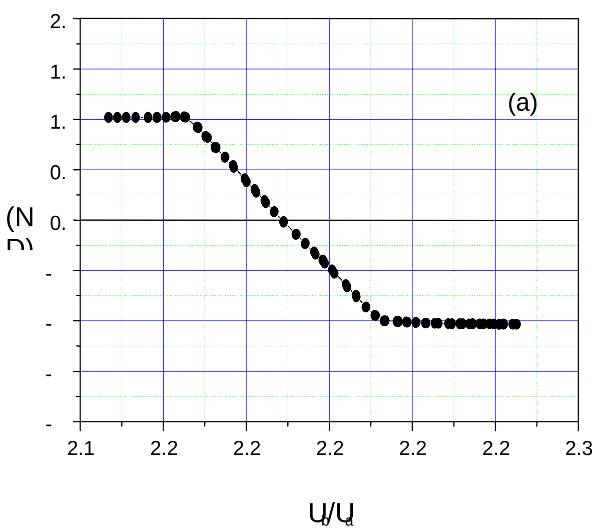

Fig. 5.6 - Dynamic curve of the bias detector with full suppression of secondary electrons.

5.5. LASER INDUCED FLUORESCENCE DIAGNOSTIC FOR TJ-II

The following main tasks were carried out in 2000:

- Maintenance of the laser
- Final setting of the new cooling system
- Improvements on the hardware of the diagnostic
- Design of the control system for this diagnostic
- Implementation and testing of the diagnostic on the TJ-II device.

5.6. DIGITAL INSTRUMENTATION FOR CONTROL AND DATA ACQUISITION

5.6.1. Introduction

The following main activities have been performed this year:

- Implementation of 3 MWords memories in the 4 channels, 250 MSPS, VME transient recorder modules
- Development of a 8 independent channels, 12 bits, 3 MSPS maximum sampling rate, 512 kWords per channel, VME transient recorder module (Fig. 5.7).
- Development of a 4 channels, 12 bits, 65 MSPS maximum sampling rate, 1 Mword per channel, VME transient recorder module (AQ4-A-B).
- End of the development of the PC version of a multiple Digital Signal Processor (DSP) system for real-time parallel processing and feedback control. This work included the design, programming and testing of the software to run on the DSPs and the development of the operation system and the interface program with the Personal Computer.
- Test of the multiple DSP system in Garching.
- Beginning of the development of the VME version of the multiple DSP system
- Development of software for operation and remote data access on an universal hardware interface system.

5.6.2. A Q4-A-B transient recorder module

AQ4-A-B is a fast transient recorder module with 4 channels with 12 bits resolution and a maximum sample rate of 65 MSPS. Each acquisition bursts can have up to 1 MSamples, since each channel has up to 1 MWord of memory (Static RAM). Other configurations can be also implemented providing maximum sampling rates of 45 and 50 MSPS and 256 kWord memory per channel.

The four channels are grouped in two blocks that have independent controls and parameters, leading to a complete independence between blocks (Fig. 5.8).

Each block has an external clock, trigger and gate signals (lemo connectors in the front panel). Software programmable parameters that define acquisition are also independent between blocks.

Depict the independence between blocks there is the possibility of locking acquisitions of both blocks to be synchronous, interleaved or sequential.

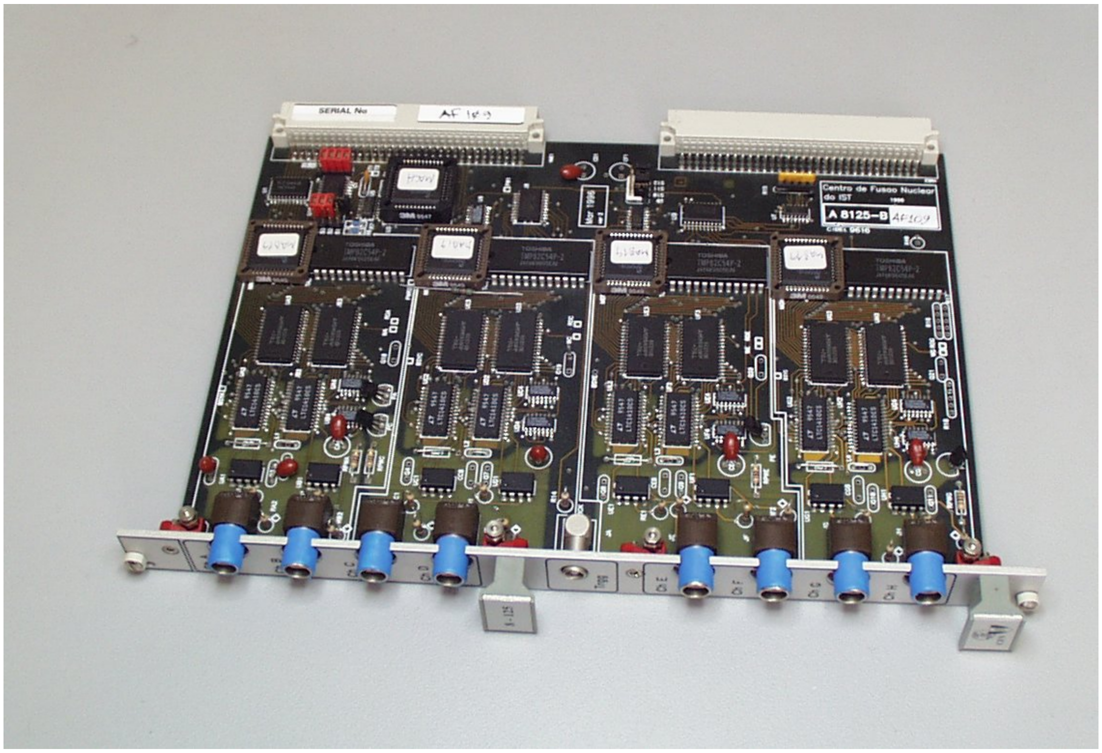

Fig. 5.7 – View of the 3 MSPS transient recorder module

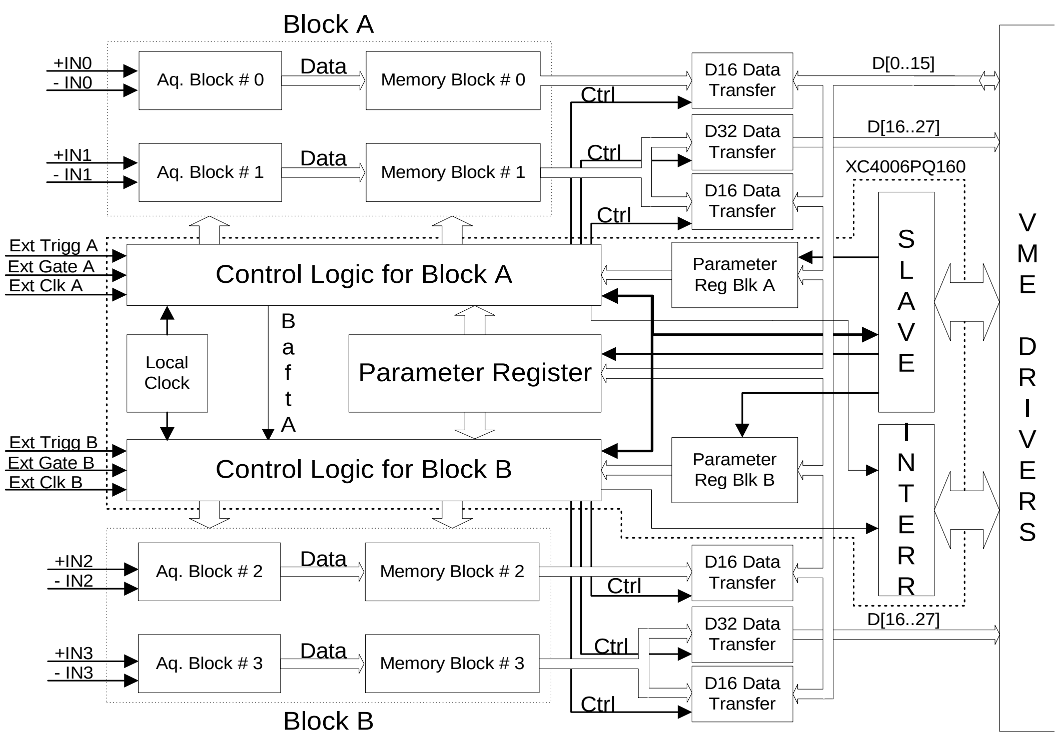

Fig. 5.8 – Block diagram of AQ4-A-B VME module

Channels of a block are completely synchronous during acquisition, but can be read independently (D16 VME data transfers) or simultaneously (D32 VME data transfers).

5.7. WIGNER DISTRIBUTIONS FOR TIME-FREQUENCY ANALYSIS OF FUSION PLASMA SIGNALS

The introduction of the Wigner distribution function in Physics occurred rather early, just a few years after the birth of quantum mechanics. The original concept, which was then envisaged as a practical tool to study quantum corrections to classical statistical mechanics, is the quantum analogue of a classical phase-space density. Today, more than six decades past, the Wigner distribution is a well-established (although advanced) concept that continues to raise interest and being applied to novel situations. It remains the subject of research in different areas, such as quantum mechanics, optics, wave physics, and time-frequency analysis.

In the work reported here, three discrete Wigner distributions have been considered as tools for the time-frequency analysis of non-stationary fusion plasma signals. They are intended to provide better results than the commonly used tools, namely the spectrogram, which remains the workhorse of time-frequency analysis. Two of these distributions were introduced in the field of signal processing.

The simplest one is due to Claasen and Mecklenbraüker. For a signal $s(n)$, where n is the sample number, it has the form:

$$W^{CM-I}(n, \theta) \equiv \frac{1}{\pi} \sum_{k} s(n+k) s^{*}(n-k) \times \exp(-i 2 k \theta). \tag{5.3}$$

The normalized frequency θ is defined as $\theta \equiv 2\pi f / f_S$, f_S being the sampling rate at which the discrete values $s(n)$ have been acquired. This distribution has a notorious drawback: the existence of aliasing whenever the spectrum of the analysed signal is not zero above $f = f_S/4$ — notice that in standard Fourier analysis the aliasing limit is twice this value, i.e., half the sampling frequency.

The same Claasen and Mecklenbraüker later avoided this shortcoming with the introduction of an improved, alias-free discrete Wigner distribution:

$$W^{CM-II}(n, \theta) \equiv \frac{1}{2\pi} \sum_{k,l} s(k) s^{*}(l) \times \frac{\sin\left[2\left(n - \frac{k+l}{2}\right)(\pi - |\theta|)\right]}{\left(n - \frac{k+l}{2}\right)} \exp\left[-i(k-l)\theta\right]. \tag{5.4}$$

The presence of a double summation in $W^{CM-II}(n, \theta)$ makes it unattractive from the computational point of view, particularly when compared with $W^{CM-I}(n, \theta)$. In fact, the calculation of $W^{CM-I}(n, \theta)$ practically resumes itself to the evaluation of a FFT.

The third Wigner distribution has been transposed to signal processing from the formally equivalent field of quantum mechanics. It has the following form:

$$W^{BMW}(n, \theta) \equiv \frac{1}{2\pi} \sum_{k,l} s(k) s^{*}(l) \times \frac{\sin\left[\left(n - \frac{k+l}{2}\right)\pi\right]}{\left(n - \frac{k+l}{2}\right)\pi} \exp\left[-i(k-l)\theta\right]. \tag{5.5}$$

This is the quantum-mechanical rotational Wigner distribution function. As far as signal processing is concerned, it has many desirable properties, namely being alias free.

The properties that are relevant for time-frequency analysis have been studied in detail. It has been shown that using the simplest distribution, $W^{CM-I}(n, \theta)$ is advantageous when the sampling rate is high, and aliasing does not constitute a problem. Indeed, this distribution is much easier to compute than the other two, competing in efficiency with the widely used spectrogram. Otherwise, the other two more complicated distributions $W^{CM-II}(n, \theta)$ and $W^{BMW}(n, \theta)$ should be preferred. They are alias-free and are very similar as far as the presence of cross-term related artifacts is concerned—the existence of such artifacts constituting their major shortcoming. As can be seen in Fig. 5.9, while $W^{CM-II}(n, \theta)$ is “clean” in the high-frequency region, in the case of $W^{BMW}(n, \theta)$ artifacts are considerably more localised, which may turn the interpretation of the time-frequency plane easier. In all three cases, it has been demonstrated that use of the analytic signal eliminates those artifacts that are due to interference with mirror signal components at the negative frequency region

(Fig. 5.10). In the case of $W^{CM\text{-}I}(n,\theta)$ using the analytic signal also serves the purpose of eliminating aliasing. From the two alias-free distributions $W^{BMW}(n,\theta)$ is the simplest to compute. Moreover, it has the advantage over $W^{CM\text{-}II}(n,\theta)$ of not being necessary to calculate at instants in-between samples in order to satisfy some important properties. Therefore, it should be used whenever aliasing is a problem. Fig. 5.11 shows the three distributions for a magnetic activity signal picked up by external Mirnov coils. Needless to say, the results obtained, as well as the analysis carried out, have implications also for the other fields where the Wigner distribution has been present.

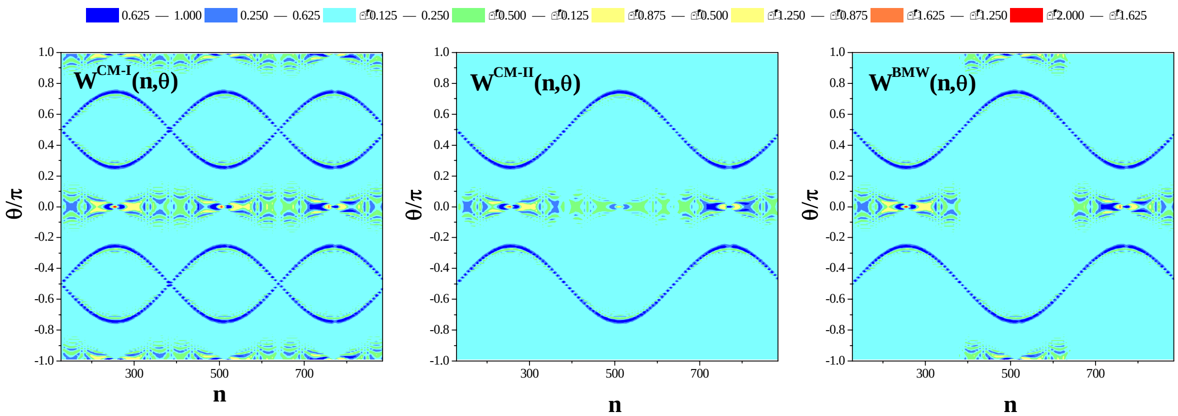

Fig. 5.9 - The distributions $W^{CM\text{-}I}(n,\theta)$, $W^{CM\text{-}II}(n,\theta)$, and $W^{BMW}(n,\theta)$, normalized to their maximum values at each instant to facilitate visualization, calculated for a two-component signal $s(n)=\cos[0.3\times\pi\times n+(0.1\times\pi)/\varpi\times\sin(\varpi\times n)]+\cos[0.7\times\pi\times n+(0.1\times\pi)/\varpi\times\sin(\varpi\times n)]$. The components oscillate with a frequency $\varpi=4\pi/N$, where the number of samples is N = 1024.

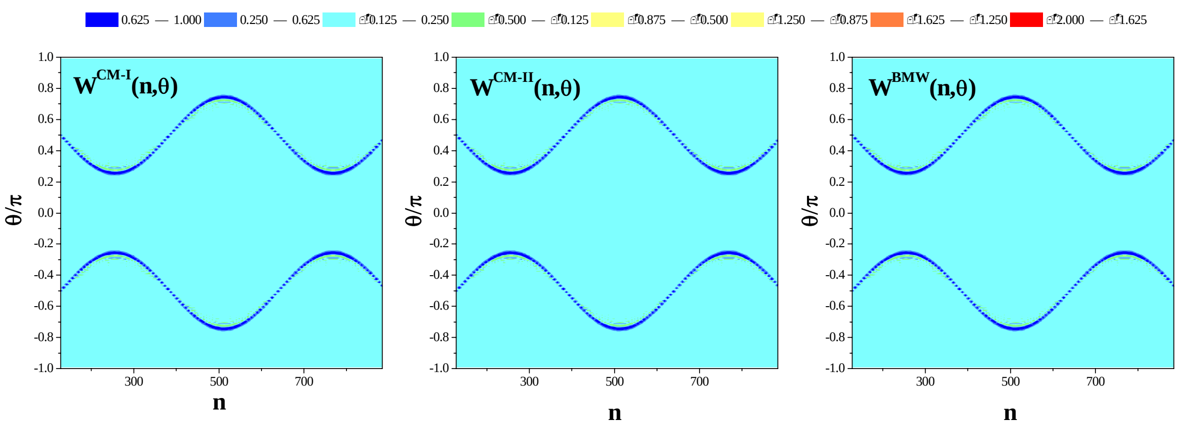

Fig. 5.10 - The distributions $W^{CM\text{-}I}(n,\theta)$, $W^{CM\text{-}II}(n,\theta)$, and $W^{BMW}(n,\theta)$, normalized to their maximum values at each instant to facilitate visualization, calculated for the analytic signal corresponding to $s(n)=\cos[0.3\times\pi\times n+(0.1\times\pi)/\varpi\times\sin(\varpi\times n)]+\cos[0.7\times\pi\times n+(0.1\times\pi)/\varpi\times\sin(\varpi\times n)]$. The components oscillate with a frequency $\varpi=4\pi/N$ where the number of samples is N = 1024.

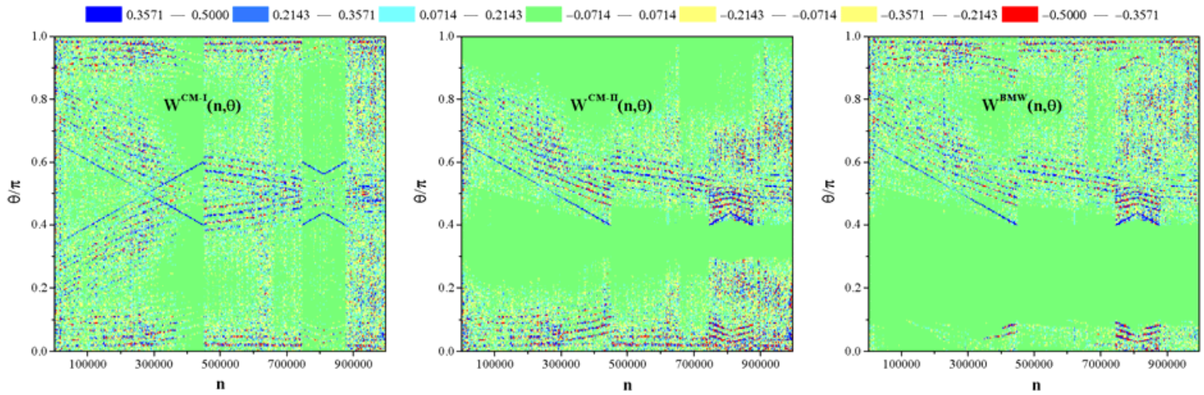

Fig. 5.11 - The distributions $W^{CM-I}(n,\theta)$, $W^{CM-II}(n,\theta)$, *and* $W^{BMW}(n,\theta)$, *normalized to their maximum values at each instant to facilitate visualization, calculated for a magnetic activity signal picked up by external Mirnov coils. The signal is made of 1 million samples, which results of sampling during 1 s with a sampling rate of 1 MHz. The value* $\theta/\pi=1$ *corresponds to half the sampling frequency, that is, 500 kHz.*